An eight-year-long low-frequency earthquake catalog for Southern Cascadia

Ariane Ducellier[1], **Kenneth Creager**[1]

[1]University of Washington

Key Points:

- We establish an eight-year-long low-frequency earthquake catalog for southern Cascadia.
- Families from the subduction zone are mainly active during the big tremor events, with down dip families more active than up dip families.
- LFE activity is sensitive to tidal stress changes.

Corresponding author: Ariane Ducellier, ducela@uw.edu

Abstract

Low-frequency earthquakes (LFEs) are small magnitude earthquakes, with typical magnitude less than 2, and reduced amplitudes at frequencies greater than 10 Hz relative to ordinary small earthquakes. Their occurrence is often associated with tectonic tremor and slow slip events along the plate boundary in subduction zones and occasionally transform fault zones. They are usually grouped into families of events, with all the earthquakes of a given family originating from the same small patch on the plate interface and recurring more or less episodically in a bursty manner. In this study, we extend the LFE catalog obtained by Plourde et al. (2015) during an episode of high tremor activity in April 2008, to the 8-year period 2004-2011. All of the tremor in the Boyarko et al. (2015) catalog south of 42 degrees North has associated LFE activity, but we have identified several other, mostly smaller, clusters of LFEs, and extend their catalog forward and backward by a total of about 3 years. As in northern Cascadia, the down-dip LFE families have recurrence intervals several times smaller than the up-dip families. For the April, 2008 Episodic Tremor and Slip event, the best recorded LFE families exhibit a strong tidal Coulomb stress sensitivity starting 1.5 days after the rupture front passes by each LFE family. The southernmost LFE family, which has been interpreted to be on the subduction plate boundary, near the up-dip limit of tremor, has a very short recurrence time. Also, these LFEs tend to occur during times when predicted tidal Coulomb stress is discouraging slip on the plate boundary. Both observations suggest this LFE family may be on a different fault.

Plain language summary

Low-frequency earthquakes (LFEs) are small magnitude earthquakes, with typical magnitude less than 2, and reduced amplitudes at frequencies greater than 10 Hz relative to ordinary small earthquakes. Their occurrence is often associated with tectonic tremor and slow slip events along the plate boundary in subduction zones and occasionally transform fault zones. They are usually grouped into families of events, with all the earthquakes of a given family originating from the same small patch on the plate interface and recurring more or less episodically in a bursty manner. In this study, we extend the LFE catalog obtained by Plourde et al. (2015) to the 8-year period 2004-2011. As in northern Cascadia, the down-dip LFE families have recurrence intervals smaller than the up-dip families. For the April 2008 Episodic Tremor and Slip event, the best recorded LFE families exhibit a strong tidal stress sensitivity. The southernmost LFE family, which has been interpreted to be on the subduction plate boundary has a short recurrence time. Also, these LFEs tend to occur during times when tidal stress discourages slip on the plate boundary. Both observations suggest this LFE family may be on a different fault.

1 Introduction

Tectonic tremor is a weak but persistent shaking of the Earth that has been discovered in many subduction zones and some strike-slip faults throughout the world **(Beroza & Ide, 2011)**. Tremor is observed on seismograms as apparent noise whose amplitude is modulated in time in a similar manner at stations that are dozens of kilometers apart from each other **(Obara, 2002)**. It is characterized by a long (several seconds to many minutes), low amplitude seismic signal, emergent onsets, and an absence of clear impulsive phases. Tremor can be explained as a swarm of low-frequency earthquakes (LFEs) **(Shelly et al., 2007a)**, that is small magnitude earthquakes (M $\sim$ 1) which dominant frequency is clearly low (1-10 Hz) compared with that of ordinary tiny earthquakes (up to 20 Hz). The source of the tremor and the LFEs is located on the plate boundary **(Shelly et al., 2006; Bostock et al., 2012; Audet & Kim, 2016)**, and their focal mechanisms represent shear slip on a low-angle thrust fault dipping in the same direction as the plate interface **(Ide et al., 2007; Bostock et al., 2012; Royer & Bostock, 2014)**.

LFEs are usually grouped into families of events, with all the earthquakes of a given family originating from the same small patch on the plate interface, and recurring more or less episodically in a bursty manner. In subduction zones such as Nankai and Cascadia, tectonic tremor and LFE observations are spatially and temporally correlated with slow slip observations **(Rogers & Dragert, 2003; Obara et al., 2004)**. Due to this correlation, these paired phenomena have been called Episodic Tremor and Slip (ETS).

The relatively short recurrence of slow slip and tremor events results in a rich history both in space and time and reveals potential patterns. These event histories have allowed scientists to see complete event cycles, which is typically not possible to explore in traditional earthquake catalogs. However, most of the work on LFEs has been focused on detecting LFEs during periods of high tremor activity, grouping them into families of events, and locating the source of the LFE families. Longer catalogs (several years) have been established for LFE families in Mexico (two-year long catalog by Frank et al. (2014)), the San Andreas Fault (fifteen-year-long catalog by Shelly (2017)), Washington State (five-year-long catalog by Sweet et al. (2019) and two-year-long catalog by Chestler and Creager (2017a, 2017b)), **Vancouver Island (ten-year-long catalog by Bostock et al. (2015))**, New Zealand (eight-year-long catalog by Baratin et al. (2018)), and Japan (twelve-year-long catalog by Nakamura (2017), eight-year-long catalog by Ohta and Ide (2017), **eleven-year-long catalog by ? (?), and Japan Meteorological Agency (JMA) catalog since 1999 (?, ?)**). These studies have shown that the recurrence behavior of LFE families varies a lot between seismic regions, and inside the same seismic region. In northern Washington, Sweet et al. (2019) have identified and characterized four different LFE families that span the width of the transition zone in the Cascadia Subduction Zone beneath western Washington State. They found that the LFEs swarm duration, recurrence interval, and event size decrease systematically with increasing depth. On the San Andreas Fault, Shelly (2017)) observed a large diversity of recurrence behaviors among the LFE families, from semicontinuous to highly episodic. Particularly, two families exhibited bimodal recurrence patterns (about 3 and 6 days for the first one, and about 2 and 4 days for the second one). Moreover, he observed an increase in the LFE event rate after the 2004 Parkfield earthquake.

Plourde et al. (2015)) have detected LFEs in southern Cascadia during the April 2008 ETS event using seismic data from the EarthScope Flexible Array Mendocino Experiment (FAME). They used a combination of autodetection methods and visual identification to obtain the initial templates. Then, they recovered higher signal-to-noise LFE signals using iterative network cross-correlation. They found that the LFE families on the southern Cascadia Subduction Zone were located above the plate boundary, with a large distribution of depths (28-47 km). Three additional LFE families were found on two strike-slip faults, the Maacama and Bucknell Creek faults, which are part of the San Andreas Fault zone.

When the hard work of detecting LFEs and identifying LFE families has been carried out, and enough (a few hundred) LFEs have been identified for a given family, a template waveform can be obtained by stacking all the waveforms corresponding to all the LFEs identified. Once a template is available, additional LFEs can be found by cross-correlating seismic data with the template, and assuming that an LFE is occurring whenever the value of the cross-correlation is higher than a chosen threshold. The signal-to-noise ratios are low, so LFEs can be best identified by stacking the cross-correlation functions of multiple stations. In this study, we first use the catalog established by Plourde et al. (2015) for the months of March and April 2008 to create templates for the temporary seismic stations of the FAME experiment. We then use these templates to extend the catalog to the whole period when the FAME experiment was running, between July 2007 and June 2009. Next, we use the LFE detections from the 2007-2009 period to create templates for the permanent stations of three seismic networks in northern California. These new templates allow us to extend the LFE catalog to the period 2004-2011.

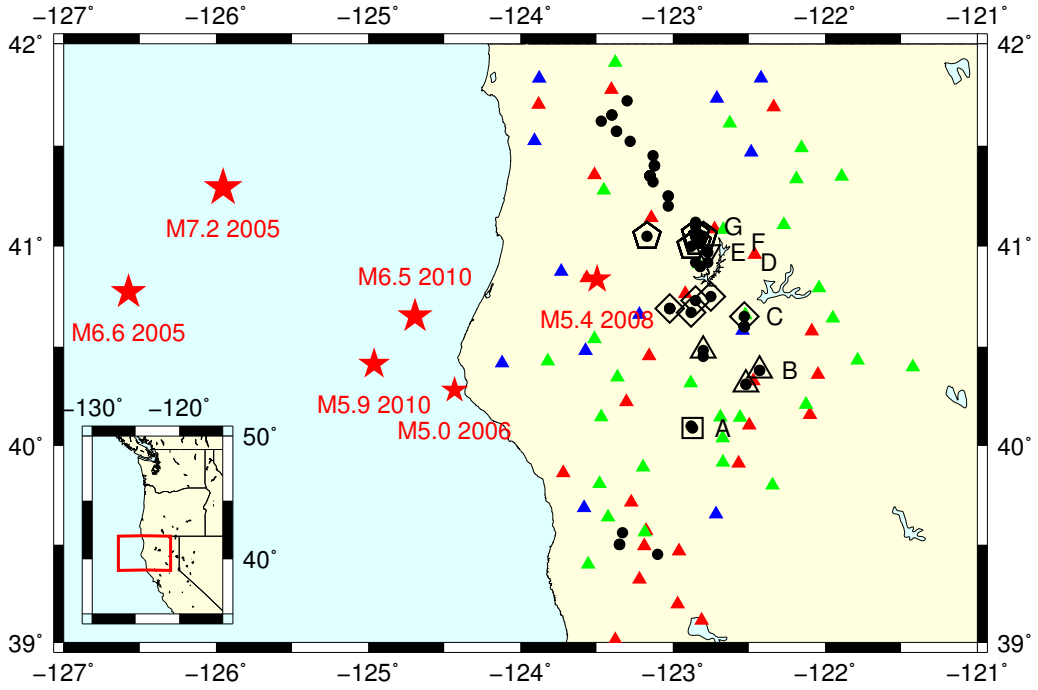

Figure 1. Map showing the location of the LFE families (back dots) and the seismic stations used in this study. Red triangles are the stations from the FAME experiment, green triangles are one-component permanent stations, blue triangles are three components permanent stations. Red stars are moderate ($M > 5$) nearby earthquakes.

2 Data

We used both seismic data from the temporary EarthScope Flexible Array Mendocino Experiment (FAME) distributed by Incorporated Research Institutions for Seismology (IRIS), and seismic data from three permanent seismic networks distributed by the Northern California Earthquake Data Center (NCEDC). The FAME network was installed in northern California between July 2007 and June 2009. The three permanent networks are Berkeley Digital Seismic Network (BK), Northern California Seismic Network (NC), and Plate Boundary Observatory Strain and Seismic Data (PB). We used both one-component and three-components seismic stations. Depending on availability, we used channels BHZ, EHZ, HHZ, or SHZ as we are mainly interested in the frequency band 1-10Hz. We restricted ourselves to seismic stations less than 100 kilometers away from the epicenter of an LFE family, as we do not expect to have good signal-to-noise ratio for stations located farther away. The complete list of seismic stations and channels used in this study is given in the Supplementary Material. Figure 1 shows a map of the locations of the LFE families, and of the locations of the seismic stations. We can see that we have a good coverage of the area, and most LFE families are surrounded by several seismic stations.

Plourde et al. (2015) have kindly shared their LFE catalog with us. For each of 66 LFE families they provided hypocentral locations, lists of stations and channels used to detect LFEs, and the timing of all LFE detections. Plourde et al. (2015) have later reduced the number of LFE families to 37, by grouping together families with many common detections, but we chose to use the initial detections to extend the catalog. Using this dataset, we have created LFE templates for each LFE family and each seismic station and channel. For a given LFE family, a given station and a given channel, we downloaded an 80-second-long seismic waveform starting 10 seconds before the LFE detection time, we detrended the data, tapered the first and last 5 seconds of the data with a Hann window, removed the instrument response, bandpassed filter between 1.5 and 9 Hz, resampled the data to 20 Hz, and cut the first and last 10 seconds of data to obtain a one-minute-long template. All these preprocessing operations are done with the Python package obspy. We then linearly stacked all the waveforms after normalizing each waveform with the root mean square (RMS) to obtain a waveform template for each station and each channel.

3 Method

We used a matched-filter algorithm to detect LFEs. For a given LFE family, we download one hour of seismic data. Then for each station and each channel, we cross-correlate the one-hour long signal with the one-minute-long template for the given station and channel. We scale the correlation coefficient by the standard deviation so the value is 1 if the correlation is perfect. As the signal-to-noise ratio of the seismic data is low, we may not see obvious peaks in the cross-correlation signal. However, if we stack the cross-correlation signals for all the channels and all the stations, we can see peaks appearing. Whenever the value of the average cross-correlation is higher than a threshold (we chose a threshold equal to eight times the median absolute deviation of the stacked cross-correlation **as was done by Shelly et al. (2007a)**), we inferred that there is an LFE. As two peaks separated by a short period of time may actually correspond to the same LFE, we kept only LFEs that are separated by at least one second and, when two LFEs are separated by less than one second, we keep only the one with the higher value of the stacked cross-correlation.

We first looked for LFEs during the months of March and April 2008, which correspond to the period covered by the catalog from Plourde et al. (2015), and compared our detections with the initial detections from the original catalog of 66 families. For 19 families, we recovered all the LFE detections initially present in the Plourde et al. (2015)'s catalog. For 61 families, we recovered more than 90 % of the initial LFE detections. We also added 74 % more LFEs to the catalog, but most of added LFEs have a low cross-correlation value and may be false detections. Figure 2 shows the cross-correlation values for the LFEs in the original catalog, and for the LFEs that we added to the catalog for family E (inverted triangle in Figure 1).

We then looked for LFEs during the period from July 2007 to June 2009, which correspond to the period when the FAME experiment was operating. Using a threshold equal to eight times the median absolute deviation of the stacked cross-correlation may produce false detections, therefore we filtered the LFE detection times before visualizing the two-year-long catalog. As the number of seismic stations recording may change with time as the stations were progressively installed during Summer and Fall 2007, and then progressively removed during May and June 2009, we kept only LFE detections for which the product of the cross-correlation value by the number of stations recording at that time is higher than a threshold. The threshold is thus different for each LFE family. The resulting LFE catalog for the period 2007-2009 is shown in Figure 3. For comparison, we also plotted the tremor detection times from Boyarko et al. (2015).

We note that there is a good spatial and temporal agreement between tremor and LFEs, with LFEs detected during the main tremor episodes. Additional small LFE episodes are also detected between bigger tremor episodes. The LFE families located south on

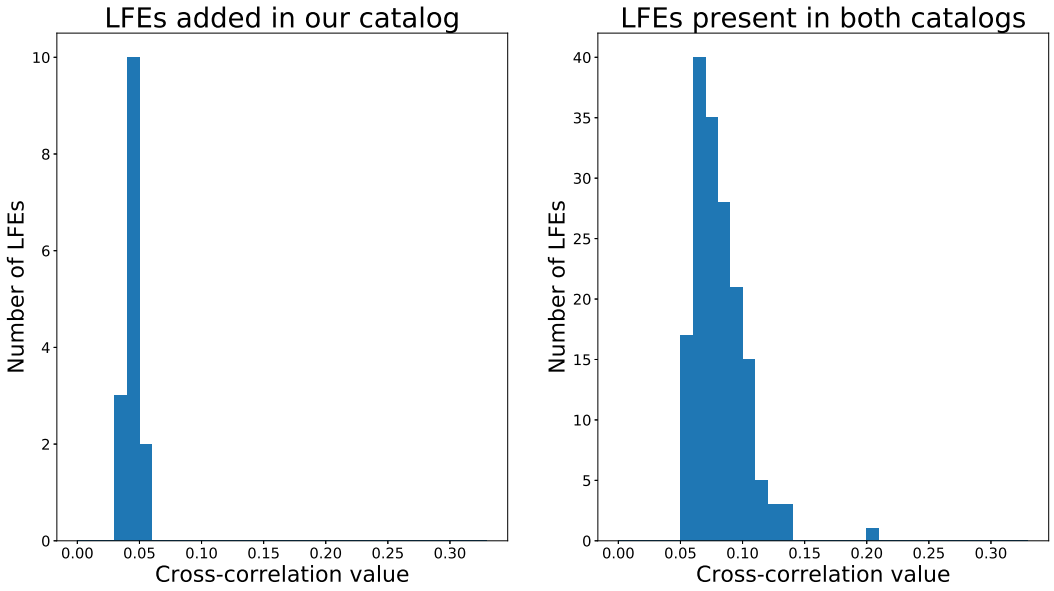

Figure 2. Cross-correlation values for LFEs added in the catalog for family E (inverted triangle in Figure 1) (left) and cross-correlation values for LFEs in the original catalog from Plourde et al. (2015) (right). There were no missing LFEs for this family.

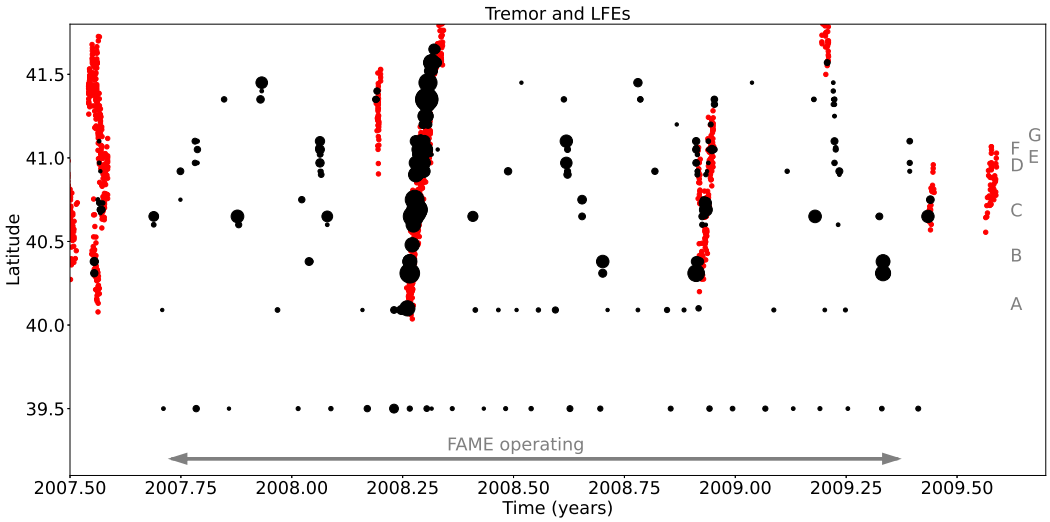

Figure 3. LFE and tremor detections as a function of time and latitude. Red dots represent tremor detections from the catalog of Boyarko et al. (2015). Black dots represent days where LFEs are detected for a given LFE family. The size of the black dots are proportional to the number of LFEs detected during this day. The double-headed grey arrow represents the time period when the FAME experiment was operating at full capacity. LFE families south of 40 N latitude are on the San Andreas fault system. For clarity, we do not show the LFEs for the days when there are less than three LFEs.

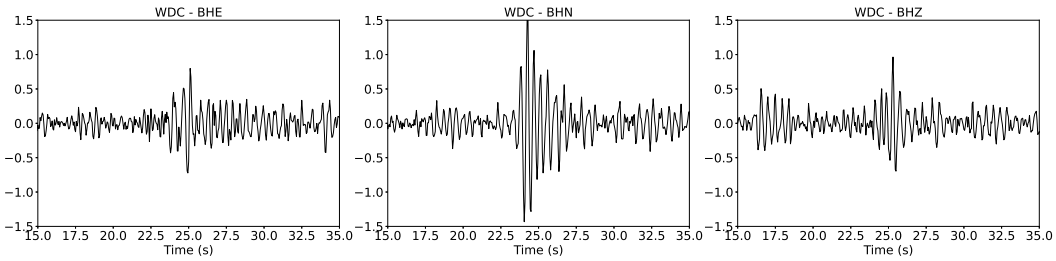

Figure 4. Low-frequency earthquake template for station WDC and family A (square in Figure 1) for the three channels BHE, BHN and BHZ (left to right). We can clearly see a P-wave arrival and an S-wave arrival about 7 seconds later. The P-wave has a higher amplitude on the vertical component, and the S-wave has a higher amplitude on the horizontal components.

the strike-slip fault from the San Andreas Fault system have much shorter recurrence intervals than the LFE families located on the subduction zone. Additionally, one LFE family located on the southern end of the subduction zone has also shorter recurrence intervals than families located farther north, and behaves more similarly to the strike-slip fault families.

We then used the LFE detections from the 2007-2009 catalog to make new templates for the permanent stations of the three seismic networks: Berkeley Digital Seismic Network (BK), Northern California Seismic Network (NC), and Plate Boundary Observatory Strain and Seismic Data (PB). For a given LFE family, we took the 150 LFE detection times with the best cross-correlation value, we downloaded one minute of seismic data around each detection, and linearly stacked the waveforms to obtain the templates. We looked for templates for both one-component stations and three-component stations.

For most families, we find that we can obtain good templates with signal-to-noise ratio for several stations. Only nine families have four or less seismic stations with good templates. Examples of templates are given in Figure 4 for station WDC and family A (square in Figure 1). To obtain the above catalog, we used one-minute-long templates, which included noise before and after the seismic wave arrivals. To increase the cross-correlation values between the templates and the data, we thus reduced the length of the templates to 25 to 40 seconds, depending on the maximum distance from the source to the stations. We did not use stations more than 100 kilometers away from the epicenter of an LFE family, as the template would be unlikely to have a good signal-to-noise ratio. We then used this new, shorter templates for the permanent stations to make an LFE catalog for the period 2007-2009.

4 Results

Once we have obtained a catalog for the period 2007-2009 using the data from the permanent seismic networks, we compare the LFE detections between the two catalogs: the FAME catalog (obtained with data from the FAME experiment) and the networks catalog (obtained from data from the permanent networks). As we may have many false detections, we try to eliminate some of them by assuming that LFEs present in both catalogs are always true detections. Then we define two thresholds: the first threshold is chosen such that at least half the LFE detections above the threshold in the FAME catalog are also in the network catalog, the second threshold is chosen such that at least half the LFE detections above the threshold in the network catalog are also in the FAME catalog. If we filter the catalogs and keep only detections above the thresholds, we are now confident that at least half of the LFE detections are true detections. As the number of stations recording may vary over time (especially for the network catalog), we keep

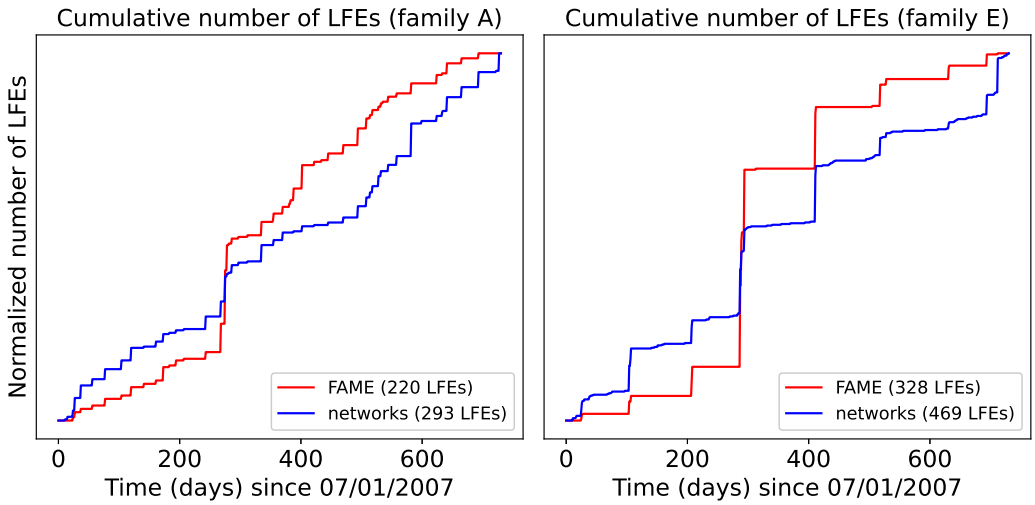

Figure 5. Normalized cumulative number of LFEs over the period July 2007-July 2009 for the FAME catalog (red) and the network catalog (blue) for family A (square in Figure 1) and family E (inverted triangle in Figure 1). The cumulative number of LFEs has been divided by the total number of LFEs so that both curves start at 0 and end at 1, in order to get a better match between the LFE bursts in both catalogs.

only the LFE detections such that the associated cross correlation multiplied by the number of channels recording at that time is higher than the threshold. Thus, if there are few stations recordings at some time, the cross correlation must be higher for the LFE to be considered as a true detection. We then compared the normalized number of LFEs obtained with the two catalogs. Examples are given in Figure 5 for families A (square in Figure 1) and E (inverted triangle in Figure 1). Although the number of LFEs during each event may not be the same, we clearly see for family E that the timing of the events are the same for both catalogs. Family A has much shorter recurrence times but most events seem to be present in both catalogs as well.

For most of the families located on the subduction zone, we obtained a good agreement between both catalogs. We eliminate two families for which too few permanent stations have good templates, and it was not possible to detect LFEs with the available templates. However, we were able to detect most LFE events even without the presence of the temporary stations from the FAME network. We are thus confident that we can detect LFEs before 2007 and after 2009. In the following, we focus on the period 2004-2011. In November 2011, several one-component stations stopped recording and the number of available stations started decreasing, which is why we did not look for LFE event after that date. The resulting LFE catalog for the period 2004-2011 is shown in Figure 6. For comparison, we also plotted the tremor detection times from Boyarko et al. (2015). Figure 7 shows the details of six big ETS events in 2004, 2005, 2006, 2007 and 2008.

5 Discussion

We were able to detect LFE events propagating from North to South or from South to North whenever there is a tremor episode in the Boyarko et al. (2015) catalog. We were also able to detect several LFE episodes in 2004-2005 before the beginning of the Boyarko et al. (2015) catalog. In particular, the LFE event in January 2005 propagating South to North from latitude 40.1 to latitude 41.2 is also present in the ETS catalog from Brudzinski and Allen (2007). We also see one LFE event in May-June 2004,

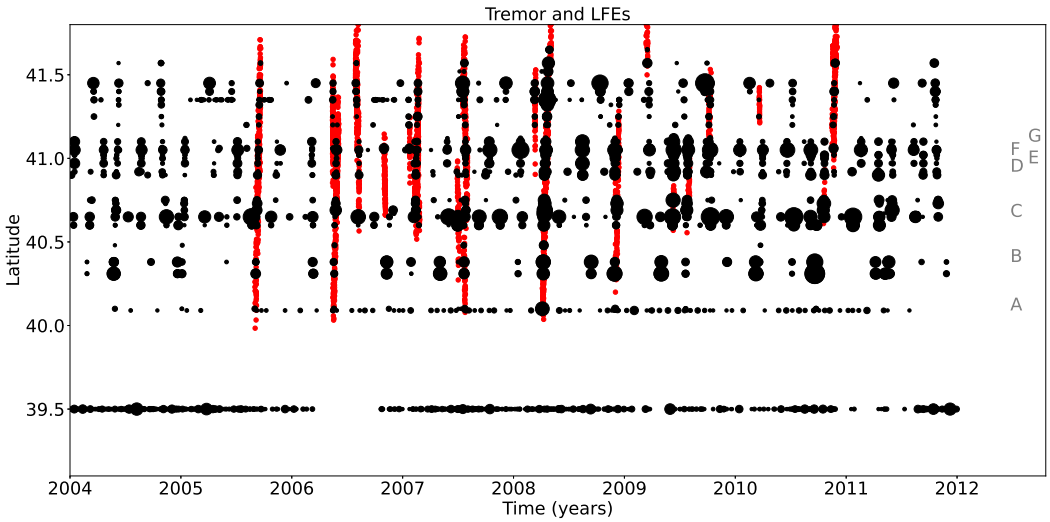

Figure 6. LFE and tremor detections as a function of time and latitude. Red dots represent tremor detections from the catalog of Boyarko et al. (2015). Black dots represent days where LFEs are detected for a given LFE family. The size of the black dots are proportional to the number of LFEs detected during this day. For clarity, we do not show the LFEs for the days when there are less than three LFEs.

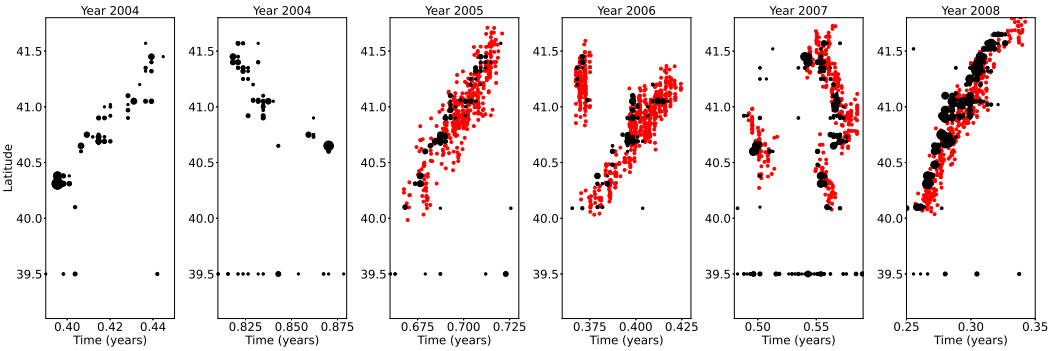

Figure 7. LFE and tremor detections as a function of time and latitude for six ETS events. Red dots represent tremor detections from the catalog of Boyarko et al. (2015). Black dots represent days where LFEs are detected for a given LFE family. The size of the black dots are proportional to the number of LFEs detected during this day. For clarity, we do not show the LFEs for the days when there are less than three LFEs.

Table 1. Main LFEs events between 2004 and 2011

Begin time	End time	Direction	Southern limit	Northern limit
End May 2004	Mid June 2004	South to North	40.1	41.6
Early November 2004	End November 2004	North to South	40.4	41.6
Early September 2005	End September 2005	South to North	40.1	41.6
Mid April 2006	End April 2006	South to North	40.1	41.5
Early July 2007	End July 2007	North to South	40.1	41.6
Early April 2008	End April 2008	South to North	40.1	41.7

Table 2. Nearby regional earthquakes between 2004 and 2011

Magnitude	Time	Latitude	Longitude	Depth (km)
7.2	2005-06-15 02:50:54	41.292N	125.953W	16.0
6.6	2005-06-17 06:21:42	40.773N	126.574W	12.0
6.5	2010-01-10 00:27:39	40.652N	124.693W	28.7
5.9	2010-02-04 20:20:21	40.412N	124.961W	23.0
5.4	2008-04-30 03:03:06	40.836N	123.497W	27.8
5.0	2006-07-19 11:41:43	40.281N	124.433W	20.1

Table 3. Teleseismic earthquakes between 2004 and 2011

Magnitude	Time	Latitude	Longitude	Depth (km)
9.1	2011-03-11 05:46:24	38.297N	142.373E	29.0
9.1	2004-12-26 00:58:53	3.295N	95.982E	30.0
8.8	2010-02-27 06:34:11	36.122S	72.898W	22.9
8.6	2005-03-28 16:09:36	2.085N	97.108E	30.0
7.9	2008-05-12 06:28:01	31.002N	103.322E	19.0

propagating South to North from latitude 40.1 to 41.6, and one LFE event in November 2004, propagating North to South from latitude 41.6 to 40.4. The first of these events is also in the ETS catalog from Brudzinski and Allen (2007). The main characteristics of the six biggest events shown in Figure 7 are given in Table 1.

It is known than tectonic tremor can be triggered by surface waves from distant and regional earthquakes, as has been observed in Cascadia (Rubinstein et al., 2009), the San Andreas (Peng et al., 2009; Guilhem et al., 2010), and Nankai **(?, ?; Han et al., 2014)**. LFE activity on the San Andreas fault also increased during several months after the 2004 Parkfield earthquake (Shelly, 2017). We looked for regional earthquakes with magnitude higher than 5 during the period covered by the catalog to verify whether this phenomenon is also observed in southern Cascadia. The characteristics of the earthquakes we looked at are given in Table 2. We also looked at distant earthquakes with large magnitude, which characteristics are given in Table 3.

Although we observe an increase in LFE activity for some families several days after the earthquakes (except the 2008 one where no activity is observed after the earthquake), it does not seem that this activity is linked to the earthquake. Indeed, the LFE events occur a few days after the earthquake and not immediately after as is the case for the Parkfield earthquake, and they affect only a few families. The reason may be due to the distance between the LFE families and the epicenters of the regional earthquakes. Indeed, for the Parkfield earthquake, an increase in LFE activity was observed for LFE families up to 45km away from the epicenter, but not farther away. Moreover, the Park-

field earthquake was more shallow (8.1km deep) than the regional earthquakes used in this study. For the 2003 M6.5 San Simeon earthquake, no increase in LFE activity in the San Andreas LFE families was observed in the hours following the earthquake. This was also a shallow earthquake (8.4km deep) but the epicenter was farther away from the LFE families (60 to 100 km). For southern Cascadia, the closest epicenter (2008) is located 50 km away from the closest LFE families. Based on what was observed for the San Andreas LFE families, this distance may be too large for a regional earthquake to trigger an increase in LFE activity. We do not see any change in LFE activity after the large teleseismic earthquakes. There was not any change in LFE activity for the San Andreas LFE families either.

In northern Cascadia, it has been observed that there is an increase in activity downdip of the plate boundary compared to up dip, both for tremor (Wech & Creager, 2011) and LFEs (Sweet et al., 2019). We want to verify whether we can see an increase of LFE activity for the downdip LFE families compared to the updip LFE families. Most families in the northern and central part of the study area are well aligned along the strike direction, however families in the southern part of the subduction zone are more distant from each other. We first look at three families aligned at latitude about 40.4N (group B, triangles in Figure 1) and show the number of LFEs per day in the left column of Figure 8. We then look at five families aligned at latitude about 40.7N (group C, diamonds in Figure 1) and show the number of LFEs per day in the middle column of Figure 8. Finally, we look at five families aligned at latitude about 41.05N (group G, pentagons in Figure 1) and show the number of LFEs per day in the right column of Figure 8. For all three sets of families, LFE events are more frequent for the easternmost family than for the westernmost family, as was also the case in northern Cascadia (Sweet et al., 2019). It is more difficult to compare event size and swarm duration as the number of stations and the quality of the templates are different from each family, and may have a strong influence on the number of LFEs detected. To summarize the findings, we plot in Figure 9 the number of LFE events as a function of the distance in the eastern direction from the upper limit of the tremor. We clearly see that the number of events increases with the down dip distance. The southernmost family A is also added in Figure 9, but does not fit the general trend.

The occurrence and amplitude of tectonic tremor can be modulated by small stress changes (about 1 kPa) associated with ocean or solid earth tides **(Shelly et al., 2007b; Houston et al., 2011; Houston, 2015)**. Sensitivity of LFE families activity to tidal stress changes has also been observed in northern Cascadia (Royer et al., 2015), and on the San Andreas fault (Thomas et al., 2012). We used calculated stresses from elastic deformations due to both water loads and body tides in the solid Earth along the Cascadia subduction zone. The stress computation is done following the method described in Houston (2015). The resulting full stress tensors are projected to normal and shear (in the plate convergence direction) stresses on the interface, as well as mean stress (one-third the tensor trace). The change in Coulomb stress (positive promotes shear failure) ΔCFF is then computed:

$$\Delta CFF = \Delta\tau + \mu\,(\Delta\sigma - B\Delta\sigma_m) \tag{1}$$

where $\Delta\tau$ is the change in shear stress on the fault plane in the slip direction, $\Delta\sigma$ is the change in fault normal stress (positive is tensile), μ is the coefficient of intrinsic friction, $\Delta\sigma_m$ is the change in mean stress and B is the Skempton's coefficient (Houston, 2015). We take the values $\mu = 0.1$ and $B = 0.5$ for the friction and the Skempton's coefficient. We then divided the values of tidal Coulomb stress change into 20 stress bins and computed for each LFE family the number of LFEs occurring at a time when the value of the stress was in a given bin. We also computed what would be the expected number of LFEs occurring if the tidal stress changes have no influence on LFE activity. As noted by Houston (2015), tremor sensitivity to stress perturbations changes during an ETS event, with an increase in sensitivity to tidal stress as slip accumulates over sev-

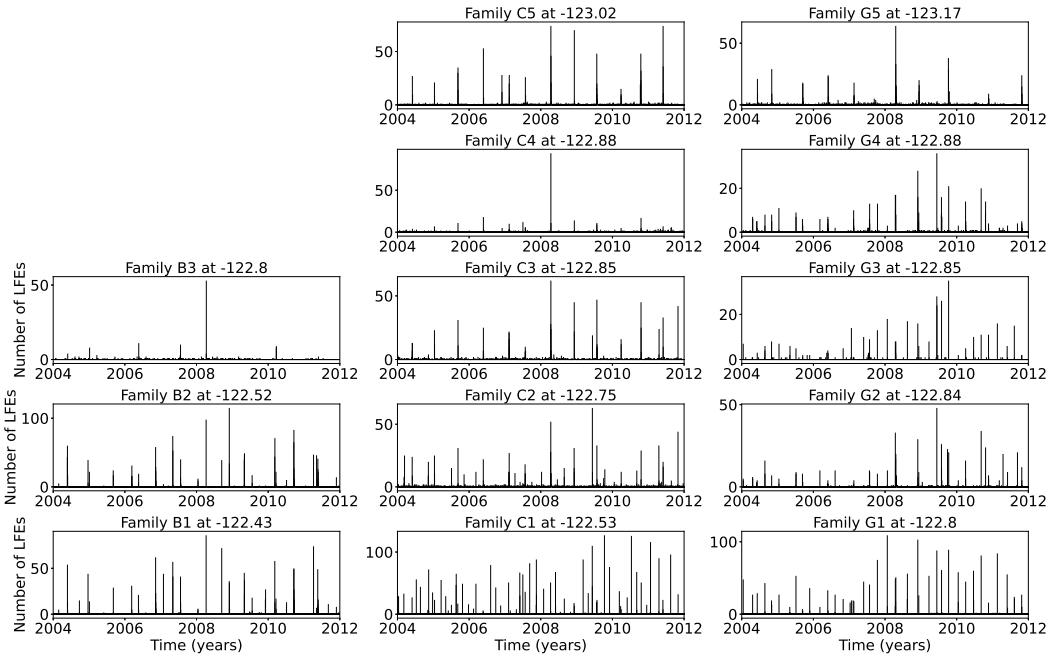

Figure 8. Left: Daily number of LFEs over the period 2004-2011 for the three LFE families in group C (triangles in Figure 1). Middle: Daily number of LFEs for the five LFE families in group D (diamonds in Figure 1). Right: Daily number of LFEs for the five LFE families in group E (pentagons in Figure 1). Down-dip families (lower rows) typically have far more LFE swarms that up-dip families (upper rows).

eral days. We thus choose to only consider the later part of the 2008 ETS event, using only LFEs that occurred between 1.5 and 11.5 days after the arrival of the tremor front. As there are only a few LFEs, it is not always obvious to see the influence of tidal stress on LFE activity. However, Figure 10 shows the number of LFEs occurring during each stress bin (blue bars) and the expected number of LFEs (black line) for six families with a relatively high number of LFEs. For most of the families, a positive Coulomb stress change (promoting shear failure) is associated with an increase in LFE activity. However, this is not the case for the southernmost LFE family A, for which a negative Coulomb stress change is associated with an increase in LFE activity. To better highlight the behavior of family A, we also consider the whole LFE catalog and plot the observed and expected number of LFEs as a function of tidal stress. We clearly see that these LFEs tend to occur during times when predicted tidal Coulomb stress is discouraging slip on the plate boundary. We hypothesize that LFE family A may not be located on the subduction zone, and may be on a different fault instead.

6 Conclusion

In this study, we used the templates obtained by Plourde et al. (2015) using data recorded by the FAME network in Northern California during an episode of high tremor activity in April 2008, and we extended their catalog to the whole two years (2007-2009) during which the seismic stations were installed. We then used the two-year-long catalog to create templates for stations from the permanent seismic networks, and used the seismic data recorded by these stations to extend the catalog before and after the FAME experiment. We observe LFEs every time that there is tectonic tremor on the tremor catalog from Boyarko et al. (2015), and several additional smaller LFE episodes. Whereas

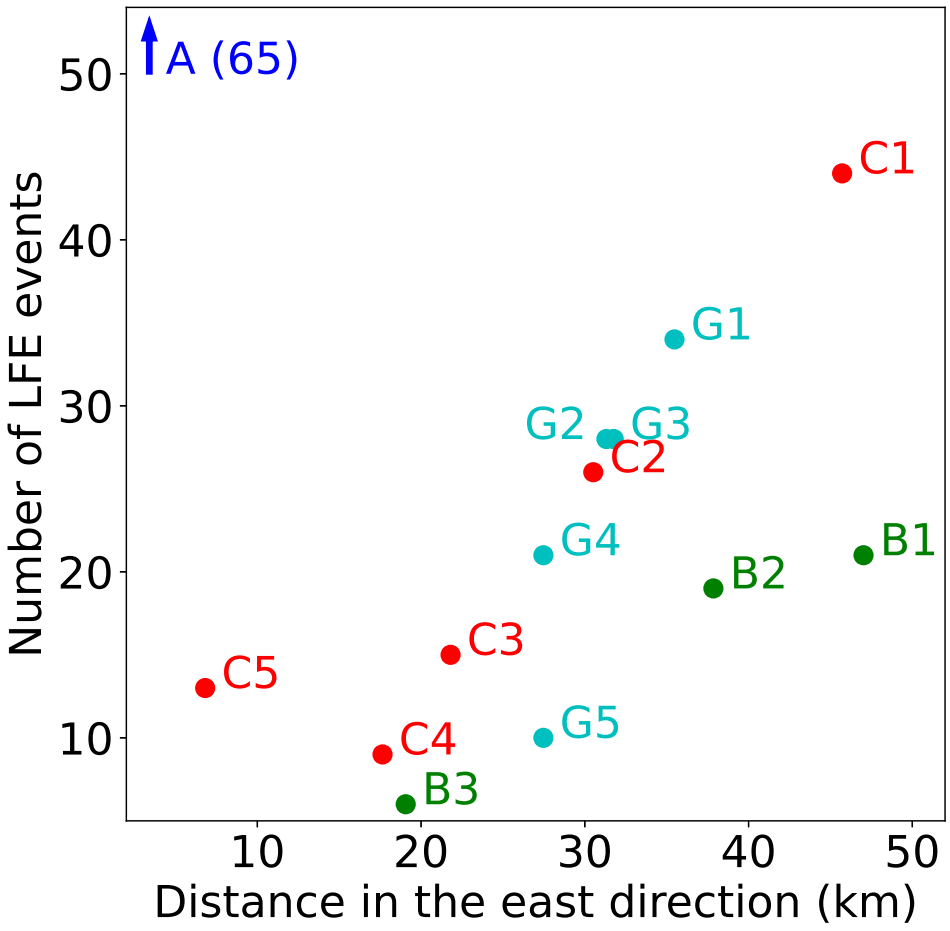

Figure 9. Number of LFE events as a function of distance in the eastern direction from the upper limit of tremor for the three LFE families in group B (triangles in Figure 1), the five LFE families in group C (diamonds in Figure 1), and the five LFE families in group G (pentagons in Figure 1). Family A (square in Figure 1) has much more LFE events and is shown by an arrow.

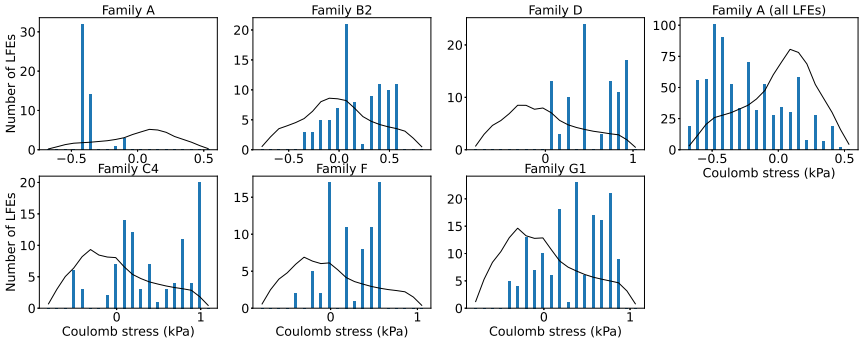

Figure 10. Number of LFEs for families A, B2, D, C4, F and G1 observed (blue bars) and expected (black line) for each stress bin of tidal Coulomb stress change.

the LFE families from the subduction zone are mainly active during the big Episodic Tremor and Slip events, the southernmost family is more active, with repeating events about once a month. Downdip families are also more active than up dip families. Tidal stress changes seem to be correlated with LFE activity in the later part of the 2008 ETS event.

Acknowledgments

The authors would like to thank A. Plourde for sharing his low-frequency earthquake catalog, D. Boyarko for sharing his tremor catalog, and H. Houston for the tidal stress calculation in the Cascadia subduction zone. This project was funded by NSF grant EAR-1358512. A.D. would like to thank the Integral Environmental Big Data Research Fund from the College of the Environment of University of Washington, which funded cloud computing resources to carry out the data analyses. The seismic recordings from the FAME experiment used for this analysis can be downloaded from the IRIS website (Alan Levander, 2007). Waveform data from the permanent networks were accessed through the Northern California Earthquake Data Center (NCEDC), doi:10.7932/NCEDC. The first figure was done using GMT (Wessel & Smith, 1991). The Python scripts used to analyze the data and make the figures can be found on the first author's Github account, accessible through Zenodo (Ducellier, 2021).

References

Alan Levander. (2007). *Seismic and geodetic investigations of mendocino triple junction dynamics.* International Federation of Digital Seismograph Networks. Retrieved from `https://www.fdsn.org/networks/detail/XQ_2007/` doi: 10.7914/SN/XQ_2007

Audet, P., & Kim, Y. (2016). Teleseismic constraints on the geological environment of deep episodic slow earthquakes in subduction zone forearcs: A review. *Tectonophysics*, *670*, 1-15.

Baratin, L., Chamberlain, C., Townend, J., & Savage, M. (2018). Focal mechanisms and inter-event times of low-frequency earthquakes reveal quasi-continuous deformation and triggered slow slip on the deep Alpine Fault. *Earth and Planetary Science Letters*, *484*, 111-123.

Beroza, G., & Ide, S. (2011). Slow earthquakes and nonvolcanic tremor. *Annu. Rev. Earth Planet. Sci.*, *39*, 271-296.

Bostock, M., Royer, A., Hearn, E., & Peacock, S. (2012). Low frequency earthquakes below southern Vancouver Island. *Geochemistry Geophysics Geosystems*, *13*, Q11007.

Bostock, M., Thomas, A., Savard, G., Chuang, L., & Rubin, A. (2015). Magnitudes and moment-duration scaling of low-frequency earthquakes beneath southern Vancouver Island. *Journal of Geophysical Research: Solid Earth*, *120*, 6329-6350.

Boyarko, D., Brudzinski, M., Porritt, R., Allen, R., & Tréhu, A. (2015). Automated detection and location of tectonic tremor along the entire Cascadia margin from 2005 to 2011. *Earth and Planetary Science Letters*, *430*, 160-170.

Brudzinski, M., & Allen, R. (2007). Segmentation in episodic tremor and slip all along Cascadia. *Geology*, *35*(10), 907-910.

Chestler, S., & Creager, K. (2017a). Evidence for a scale-limited low-frequecny earthquake source process. *Journal of Geophysical Research: Solid Earth*, *122*, 3099-3114.

Chestler, S., & Creager, K. (2017b). A model for low-frequency earthquake slip. *Geochemistry, Geophysics, Geosystems*, *18*, 4690-4708.

Ducellier, A. (2021, August). *Arianeducellier/catalog: Paper submission.* Zenodo. Retrieved from `https://doi.org/10.5281/zenodo.5168867` doi: 10.5281/zenodo.5168867

Frank, W., Shapiro, N., Husker, A., Kostoglodov, V., Romanenko, A., & Campillo, M. (2014). Using systematically characterized low-frequency earthquakes as a fault probe in Guerrero, Mexico. *Journal of Geophysical Research: Solid Earth*, *119*, 7686-7700.

Guilhem, A., Peng, Z., & Nadeau, R. (2010). High-frequency identification of non-volcanic tremor triggered by regional earthquakes. *Geophysical Research Letters*, *37*, L16309.

Han, J., Vidale, J., Houston, H., Chao, K., & Obara, K. (2014). Triggering of tremor and inferred slow slip by small earthquakes at the Nankai subduction zone in southwest Japan. *Geophysical Research Letters*, *41*, 8053-8060.

Houston, H. (2015). Low friction and fault weakening revealed by rising sensitivity of tremor to tidal stress. *Nature Geoscience*, *8*(5), 409-415.

Houston, H., Delbridge, B., Wech, A., & Creager, K. (2011). Rapid tremor reversals in Cascadia generated by a weakened plate interface. *Nature Geoscience*, *4*, 404-409.

Ide, S., Shelly, D., & Beroza, G. (2007). Mechanism of deep low frequency earthquakes: Further evidence that deep non-volcanic tremor is generated by shear slip on the plate interface. *Geophysical Research Letters*, *34*, L03308.

Nakamura, M. (2017). Distribution of low-frequency earthquakes accompanying the very low frequency earthquakes along the Ryukyu Trench. *Earth, Planets, and Space*, *69*(1), 1-17.

Obara, K. (2002). Nonvolcanic deep tremor associated with subduction in southwest Japan. *Science*, *296*(5573), 1679-1681.

Obara, K., Hirose, H., Yamamizu, F., & Kasahara, K. (2004). Episodic slow slip events accompanied by non-volcanic tremors in southwest Japan subduction zone. *Geophysical Research Letters*, *31*, L23602.

Ohta, K., & Ide, S. (2017). Resolving the detailed spatiotemporal slip evolution of deep tremor in Western Japan. *Journal of Geophysical Research: Solid Earth*, *122*(12), 10009-10036.

Peng, Z., Vidale, J., Wech, A., Nadeau, R., & Creager, K. (2009). Remote triggering of tremor along the San Andreas Fault in central California. *Journal of Geophysical Research*, *114*, B00A06.

Plourde, A., Bostock, M., Audet, P., & Thomas, A. (2015). Low-frequency earthquakes at the southern Cascadia margin. *Geophysical Research Letters*, *42*, 4849-4855.

Rogers, G., & Dragert, H. (2003). Tremor and slip on the Cascadia subduction zone: The chatter of silent slip. *Science*, *300*(5627), 1942-1943.

Royer, A., & Bostock, M. (2014). A comparative study of low frequency earthquake templates in northern Cascadia. *Earth and Planetary Science Letters*, *402*, 247-256.

Royer, A., Thomas, A., & Bostock, M. (2015). Tidal modulation and triggering of low-frequency earthquakes in northern Cascadia. *Journal of Geophysical Research Solid Earth*, *120*, 384-405.

Rubinstein, J., Gomberg, J., Vidale, J., Wech, A., Kao, H., Creager, K., & Rogers, G. (2009). Seismic wave triggering of nonvolcanic tremor, episodic tremor and slip, and earthquakes on Vancouver Island. *Journal of Geophysical Research Solid Earth*, *114*, B00A01.

Shelly, D. (2017). A 15 year catalog of more than 1 million low-frequency earthquakes: Tracking tremor and slip along the deep San Andreas Fault. *Journal of Geophysical Research: Solid Earth*, *122*, 3739-3753.

Shelly, D., Beroza, G., & Ide, S. (2007a). Non-volcanic tremor and low-frequency earthquake swarms. *Nature*, *446*, 305-307.

Shelly, D., Beroza, G., & Ide, S. (2007b). Complex evolution of transient slip derived from precise tremor locations in western Shikoku, Japan. *Geochemistry, Geophysics, Geosystems*, *8*, Q10014.

Shelly, D., Beroza, G., Ide, S., & Nakamula, S. (2006). Low-frequency earthquakes in Shikoku, Japan, and their relationship to episodic tremor and slip. *Nature*, *442*, 188-192.

Sweet, J., Creager, K., Houston, H., & Chestler, S. (2019). Variations in Cascadia low-frequency earthquake behavior with downdip distance. *Geochemistry, Geophysics, Geosystems*, *20*, 1202-1217.

Thomas, A., Bürgmann, R., Shelly, D., Beeler, N., & Rudolph, M. (2012). Tidal triggering of low frequency earthquakes near Parkfield, California: Implications for fault mechanics within the brittle-ductile transition. *Journal of Geophysical Research*, *117*, B05301.

Wech, A., & Creager, K. (2011). A continuum of stress, strength and slip in the Cascadia subduction zone. *Nature Geoscience*, *4*, 624-628.

Wessel, P., & Smith, W. H. F. (1991). Free software helps map and display data. *EOS Trans. AGU*, *72*, 441.